Subwavelength control of electromagnetic field confinement in self-similar chains of magnetoplasmonic core-shell nanostructures

M. Essone Mezeme, S. Lasquellec, and C. Brosseau[*]

Université Européenne de Bretagne, Université de Brest, Lab-STICC, CS 93837, 6 avenue Le Gorgeu,
F-29238 Brest Cedex 3, France

We apply first-principles methodology to study the spatial localization of electric field enhancement at plasmonic resonance and magnetic field enhancement at gyroresonance in a self-similar chain of magnetoplasmonic core-shell nanostructures (MCSNs). Localized regions of high electric and magnetic fields in the vicinity of metal nanostructures can be created in a controlled manner by adjusting the physical parameters characterizing this system and the polarization of the external harmonic excitations. We demonstrate the high degree of control achieved on electric field confinement, of the order of 10^3, down to a feature size of $\lambda/1000$ in self-similar chains of MCSNs, where λ denotes the free space wavelength of the resonant excitation. We also compare our findings with recent investigations in related plasmonic nanostructures.

I. INTRODUCTION

The past decade saw the discovery of an array of remarkable properties related to surface-plasmon resonances in metallic nanostructures and their aggregates [1–5]. Among these were optical nanoantennas [4, 6–8], metallic nanowires [9], and chains of resonantly coupled metallic nanoparticles [5, 10–12]. These discoveries initiated the development of plasmonics as a major research field. The recent reviews of Maier [1] and Raether [2] summarize the broad range of experimental techniques applied to plasmonic materials. Very recent reports demonstrate that magnetoplasmonic core-shell nanostructures (MCSNs) have the ability to create extremely high electric fields (hot spots), for example, at the apex of a sharp tip [13,14]. MCSNs are expected to be very significant in the context of optical antennas for at least two reasons: (i) The use of magnetic and optical imaging technologies with different penetration depths and information components is important; (ii) the plasmonic properties are significantly influenced by the permittivity of the magnetic phase [5]. The recent discovery by Li, Stockman, and Bergman (LSB) of a nanolens effect associated with a self-similar linear chain of several metal nanospheres [9] has reenergized efforts to understand the fascinating phenomenon of nanosphere cascade nanolens yielding electric field enhancement (F_E) in the nanogap between two nanoparticles which can exceed the excitation field by a factor of 10^3. The locations of the hot spots depend mainly on the geometry of the plasmonic (metal) phase. All of these factors motivate the need for accurate numerical methods that can provide a full electromagnetic description of MCSNs of arbitrary shape and size, subject to a complex dielectric environment, thus allowing for the theoretical design and optimization of novel optical antennas. It is therefore significant to understand if and how the local magnetic and electric fields are sensitive to relevant geometric parameters in self-similar systems built of a few MCSNs.

In this work we employ first-principles simulations performed within finite element (FE) modeling to investigate the effective electromagnetic behavior of a simple model of self-similar MCSNs. In our approach, we study systematically the frequency dependence of the effective (relative) magnetic permeability $\mu = \mu' - j\mu''$ and permittivity $\varepsilon = \varepsilon' - j\varepsilon''$, up to five iterations of the MCSNs, as a function of both geometric parameters and polarization of the electromagnetic field. Our results also suggest that the spatial extent of the F_E at plasmonic resonance (PLR) and magnetic field enhancement (F_M) at gyroresonance (GYR) scales as $\lambda/1000$, where λ denotes the free space wavelength of the resonant excitation. We demonstrate how the F_E and F_M are sensitive to polarization of the exciting electromagnetic field and geometric control parameters. Our calculations are in qualitative agreement with the recent data reported by Bidault *et al*. [15], who found that the maximum field is localized at the surface of the smaller particle, that is, highest curvature, of a nanoparticle assembly.

II. MODEL AND DETAILS OF THE CALCULATIONS

During our work on this topic, we noticed that calculations of the electromagnetic response of MCSNs on the basis of first-principles calculations are sparse. Recently, we provided a systematic survey of ε and μ of MCSNs, therefore filling partly the above mentioned gap in the existing literature [13,14]. The simulation geometry of our system is shown in Fig. 1. Specifically, we consider a MCSN composed of a magnetic core (gray area, phase 3) which is coated by a plasmonic shell [blue area (light gray ring), phase 2]. The dielectric properties of the embedding medium (phase 1) can be assimilated to water. We assume ideally smooth interfaces between rigid phases. The MCSNs are obtained using scaled-down copies of an initial geometry. A recursive algorithm, that is, $R_{i+1} = kR_i$, $e_i = tR_i$, and $d_{i,i+1} = \ell R_{i+1}$, can be developed to generate any occurrence of such self-similarity for a given iteration i. The self-similar MCSNs can be implemented through the three parameters shown in Fig. 1. Here, R_i denotes the radius of the ith iteration, e_i is the thickness of the ith iteration, and i parametrizes the iteration process (as illustrated in Fig. 1). In all simulations

─────────
[*]FAX: 33-2-98 01 61 31; brosseau@univ-brest.fr; also affiliated with Département de Physique, Université de Bretagne Occidentale.
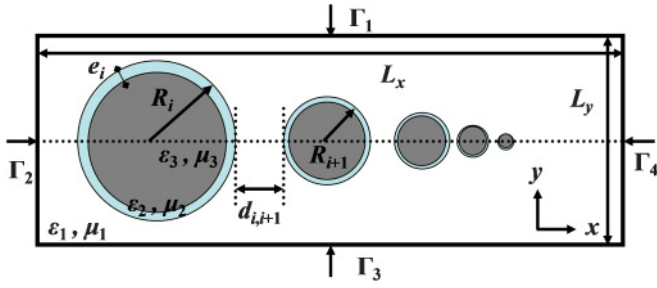
FIG. 1. (Color online) Schematic illustration (not to scale) of the simulated cell employed to determine the effective complex permittivity and magnetic permeability of our model three-phase system consisting of a set of CS nanostructures in close proximity. The numerical parameters for calculations were $R_1 = 405$ nm, $L_x = 2600$ nm, and $L_y = 910$ nm. This three-phase system consists of two concentric circular cylinders of infinite extent, that is, the shell [phase 2, blue (light gray)] and the core (phase 3, gray) embedded in a nonabsorbing surrounding medium (phase 1). The $(i + 1)$th cylinder has outer radius $R_{i+1} = kR_i$. The shell medium is supposed to have permittivity $\varepsilon_2 = \varepsilon_2' - j\varepsilon_2''$ and magnetic permeability $\mu_2 = 1$, the core medium has permittivity $\varepsilon_3 = \varepsilon_3' - j\varepsilon_3''$ and magnetic permeability $\mu_3 = \mu_3' - j\mu_3''$, and the host's permittivity reads $\varepsilon_1 = \varepsilon_1' - j/\omega\varepsilon_0$, with $\varepsilon_1' = 80$ ($\varepsilon_1' = 1.77$) in the GHz (THz) range of frequencies [14] and magnetic permeability $\mu_1 = 1$.

the radius corresponding to the first iteration is held fixed at $R_1 = 405$ nm. The choice of this parameter and the number of iterations should be consistent with the overall area $L_x L_y$ of the cell. Clearly, the process cannot be carried up to a high number of iterations. In this paper, we were able to perform calculations up to five iterations over wide range of geometric parameters: $k = 1/3 - 2/3$, $t = 0.2$–0.3, and $\ell = 0.3 - 0.6$.

To set the stage for a proper calculation of the effective electromagnetic parameters using our model, we begin with some preliminaries. Simulations were carried out in a rectangular-shaped cell containing the self-similar chain of MCSNs as shown in Fig. 1. Material property parameters used in the simulations, such as permittivity and magnetic permeability, some of which are frequency dependent, are taken from Refs. [16,17]. Gold and silver are chosen as model shell materials and were modeled using a Drude model. For Au, plasma frequency $\omega_p/2\pi = 2175$ THz, collision frequency $\omega_c/2\pi = 6.5$ THz [16], and $\varepsilon_\infty' = 7$. For Ag, plasma frequency $\omega_p/2\pi = 2149$ THz, collision frequency $\omega_c/2\pi = 12.2$ THz [16], and $\varepsilon_\infty' = 2.48$. The magnetically active part of the CS structure is the core phase for which the Landau-Lifshitz-Gilbert model provides a realistic description of the dynamics of magnetization in an external magnetic field [17]. The material properties of the pure core (Fe$_3$O$_4$) were as follows: plasma frequency $\omega_p/2\pi = 7.26$ THz, collision frequency $\omega_c/2\pi = 2$ THz, $\varepsilon_\infty' = 4.73$, gyromagnetic ratio of the electron $\gamma/2\pi = 2.8$ GHz/kOe, saturation magnetization $M_S = 70$ emu g^{-1}, GYR frequency $\omega_R/2\pi = 4.5$ GHz, and Gilbert damping constant $\alpha = 10^{-2}$ [17]. A comment should be made on the tacit quasistatic assumption that underlies the current calculations. Magnetic oxide and nonmagnetic metal materials are defined by an inhomogeneous permittivity, but at sufficiently long wavelengths they can be accurately modeled by homogeneous constitutive parameters that can

be very different from the constituent materials. The validity of this long-wavelength behavior is rooted in the fact that all length scales must be much smaller than the wavelength of radiation. We use a continuum modeling approach built upon constitutive equations which can capture the material behavior on experimentally relevant scales, that is, when the local electrical response is in terms of a position dependent permittivity. We further assume that within these linear response calculations, only linear effects are accessible to this technique; that is, the interaction of the MCSNs with the electromagnetic wave is modeled by induced electric and magnetic dipole moments. Assuming that quantum effects in the shell can be ignored, and thus that the physics described by our approach is entirely classical, sets a fundamental limiting factor for how small systems can be designed. Thus, the thickness of the metallic shell should be larger than the Fermi wavelength ($\lambda_F \approx 0.5$ nm for Au). For example, taking $k = 1/3$, $t = 0.2$, and $\ell = 0.3$, $e_4 \approx 3\lambda_F$ and $e_5 \approx \lambda_F$. We expect that the quantized character of plasmons can be significant for $i > 5$. How important is the quantum effect at large iteration numbers hinges on an effective quantum theory of the plasmonics of metallic nanoparticles and nanostructures [18,19]. Notice that the penetration depth of electromagnetic waves at optical frequencies is about 20 nm for Au. Although this conventional Drude form is often assumed to be applicable to small particles, we notice that a modification of the imaginary part of the metal phase, $\varepsilon_2(\omega)$, is sometimes assumed in the literature in order to account for the enhanced rate of electron scattering due to particle size-dependent effects [20,21], that is, when the particle size R is smaller than the mean free path in the bulk metal, conduction electrons are additionally scattered by the surface and ω_c may be modified to become size-dependent according to the specific form $\omega_c(R) = \omega_c(bulk) + v_F/R$, where v_F denotes the velocity of the electrons at the Fermi energy, that is, typically $\approx 10^6$ ms^{-1} for Au and Ag [22–24]. A recent analysis of the influence of a size-dependent permittivity of small silver particles was performed by Xu [21]. His analysis shows that within the assumption of a specific value of the electron mean path of the electron-surface collision the real part of the modified permittivity is not much changed. However, its imaginary part increases of about 70% compared to the bulk value. At this point, a crucial question is whether the correction due to spatial nonlocality has a profound impact on the effective permittivity. To answer this, we have calculated the values of ε' and ε'' for a range of k, t, and ℓ values by taking into account this correction to the bulk collision frequency. For the example $k = 1/3$, $t = 0.1$, and $\ell = 0.3$, differences of 6% in the values of ε' and of 11% in the values of ε'' were evidenced at PLR for the fifth iteration of the MCSNs, compared with the case when this correction is ignored. As in [25], this suggests that F_E may be affected only slightly up to five iterations of the MCSN array. Thus, as in previous work [3], [9], such electron confinement in conducting nanoparticle will be neglected for our purposes.

In the remainder of this work we show results of simulations which have been obtained using the code package COMSOL MULTIPHYSICS, a commercial program that uses FE methods to solve partial differential equations [24]. Assuming an exp(–jωt) time dependence throughout, we are able to extract ε and μ within a FE framework using the method proposed

in Refs. [13] and [14]. When E and H are directed along the x axis, the boundary conditions used were $V = E_0 L_x$ (V) on Γ_2, $V = 0$ V on Γ_4, and $\partial V/\partial n = 0$ on Γ_1 and Γ_3 and $J = J_0$ (A m^{-2}) on Γ_1, $J = -J_0$ (A m^{-2}) on Γ_3, and $H \times n = 0$ on Γ_2 and Γ_4. When E and H are directed along the y axis, the boundary conditions used were $V = E_0 L_y$ (V) on Γ_1, $V = 0$ V on Γ_3, and $\partial V/\partial n = 0$ on Γ_2 and Γ_4 and $J = J_0$ (A m^{-2}) on Γ_4, $J = -J_0$ (A m^{-2}) on Γ_2 et $H \times n = 0$ on Γ_1 and Γ_3. For our calculations, the values, $E_0 = 1$ V m^{-1} and $J_0 = 1$ A m^{-2}, were used. The simulations shown here used meshes generated by an advanced front algorithm with the COMSOL MULTIPHYSICS package, which automatically sets several parameters for the meshing. For all the modeling presented here we used a personal computer with a Pentium IV processor (3 GHz). Details of this procedure have been presented elsewhere [13,14]. The consistency and validation of this procedure was verified by agreement (not shown) of our calculations with those obtained from Kramers-Kronig causality relationships [14].

III. RESULTS AND DISCUSSION

The MCSNs studied here have profound polarization-dependent properties. Figure 2 shows calculations of $\varepsilon(\omega)$ and $\mu(\omega)$ when the electric field is oriented along the x axis and the magnetic field is directed along the y axis. There are two main observations. First, it is significant that the different iterations of the MCSNs all lead to quantitatively close results for μ shown in Fig. 2(a). Second, we observe from the ε data of Fig. 2(b) a complicated spectral structure, both in magnitude and in line shape, of the PLR as the iteration number i is increased: i more or less separated resonance peaks arise in the visible spectra. When the magnetic field is oriented along the x axis, there is hardly any difference observed for μ' and μ'' [Fig. 3(a)]. By contrast, a profound anisotropy was found for the electric field; that is, the ε' and ε'' spectra shown in Fig. 3(b) deviate strongly from the corresponding

FIG. 3. (Color online) (a) Same as in Fig. 2 when the magnetic field is oriented along the x axis. $k = 1/3$, $t = 0.2$, and $l = 0.6$. The metal phase is assumed to be Au. (b) Same as in (a) for the effective complex permittivity. The electric field is oriented along the y axis.

spectra for the E_x polarization [Fig. 2(b)]. Remarkably, we observe the redshifting of PLR down to 2658 THz and its characteristics do not vary significantly with the different iterations considered. These observations are consistent with the recent virial analysis of depolarization factor for arbitrarily shaped inclusions [26]. Polarization can modify the optical properties of neighboring iterations, creating new resonant modes through coupling [27]. The dipolar character of this coupling is expected to affect the F_E and F_M [28,29].

The characteristic features of the PLR and GYR rely on a delicate interplay between the geometric parameters k, t, and ℓ, the intrinsic properties of the phases, and the iteration number of the MCSNs. Detailed calculations aimed at determining the iteration number dependence of the PLR in different MCSNs containing Au and Ag and values of k, t, and ℓ have been performed and the results are shown in Fig. 4. In these simulations we kept all the other computational parameters the same. There are significant variations in the
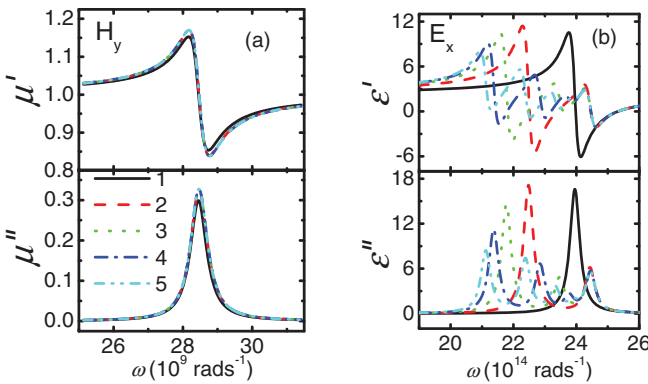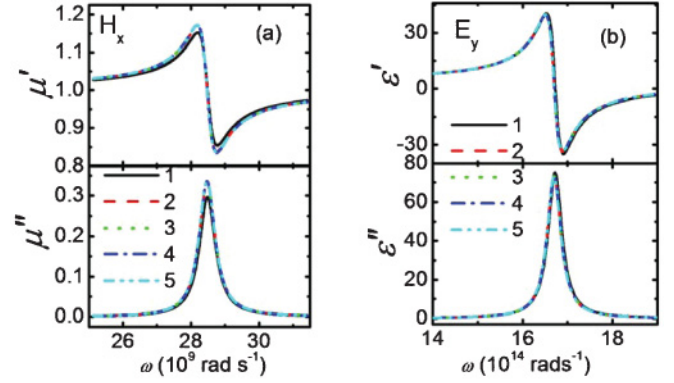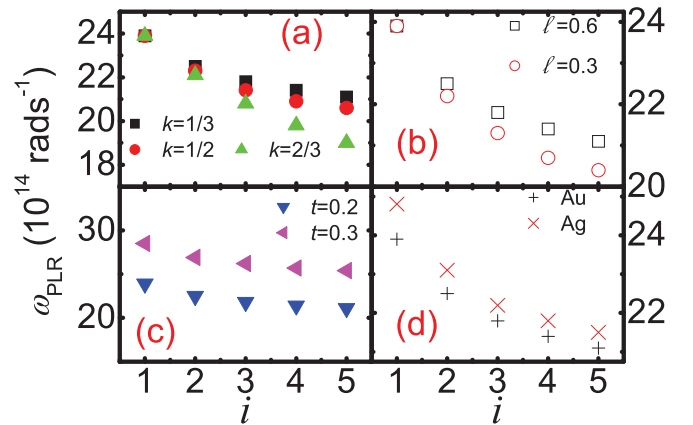

FIG. 2. (Color online) (a) Top panel: The real part, μ', of the effective complex magnetic permeability plotted as a function of the angular frequency, ω, near the GYR. The magnetic field is directed along the y axis. We also assumed that $t = 0.2$, $k = 1/3$, and $l = 0.6$. The numbers indicate the iteration numbers i. Bottom panel: Same as in the upper panel for the imaginary part of the magnetic permeability. (b) Same as in (a) for the effective complex permittivity. The metal phase is assumed to be Au. The electric field is x directed.

FIG. 4. (Color online) (a) The PLR frequency as function of the iteration number for MCSNs containing Au and different values of k with $t = 0.2$ and $l = 0.6$. E_x polarization: (b) same ($k = 1/3$, $t = 0.2$) as in (a) for two values of ℓ. The metal phase is assumed to be Au: (c) same ($k = 1/3$, $l = 0.6$) as in (a) for two values of t. The metal phase is assumed to be Au: (d) same ($k = 1/3$, $t = 0.2$, and $l = 0.6$.
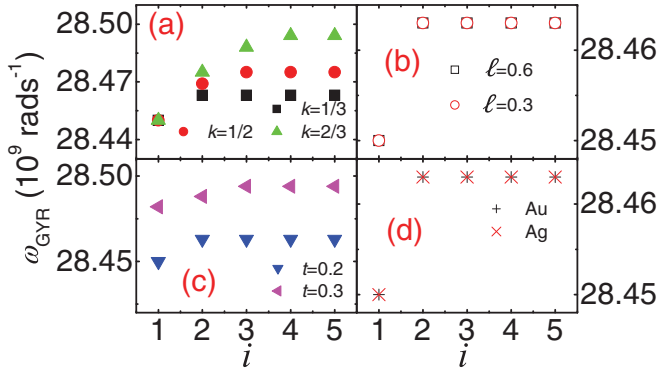
FIG. 5. (Color online) Same as in Fig. 4 for the GYR. H_y polarization. (a) $t = 0.2$, $l = 0.6$; the metal phase is assumed to be Au. (b) $k = 1/3$, $t = 0.2$; the metal phase is assumed to be Au. (c) $k = 1/3$, $l = 0.6$; the metal phase is assumed to be Au. (d) Same as in (a) for the case of Ag with $k = 1/3$, $t = 0.2$, and $l = 0.6$.

results suggesting that even small changes in the geometry of the MCSNs can have significant impact on the characteristic features of the resonances. The first point to draw from the data is the redshifting of PLR as the iteration number i is increased. There is also a general trend of decreasing the PLR frequency as the particle spacing ratio ℓ and the relative CS thickness t is decreased. Another characteristic feature is that the PLR frequency is decreased when the shell material is changed from silver to gold. We also performed GYR calculations for widely ranging geometric parameters k, t, and ℓ, and different iteration numbers. We can see that the spectral features of the GYR show only very small changes (Fig. 5), as expected.

Detailed calculations of the F_E and F_M against the iteration number (electric field along the x axis and magnetic field along the y axis) are illustrated in Figs. 6 and 7. The trends in Fig. 6 reflect the competition between the different geometric factors of the nanostructure. For the range of geometric parameter and field polarizations explored, optimum of F_E is achieved for the fifth iteration of the MCSNs, $k = 1/3$, $t = 0.5$, and $\ell = 0.6$, and the metal phase of the shell being gold. We note that previous calculations [15] corroborate qualitatively the monotonic decrease in F_E, seen in Fig. 6(b), as particle spacing is increased. It should be noted, however,
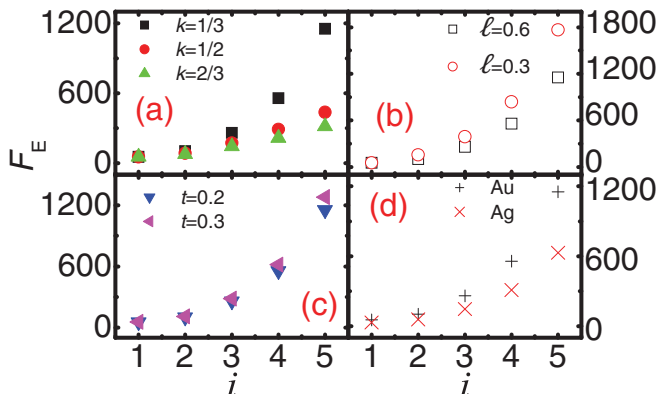

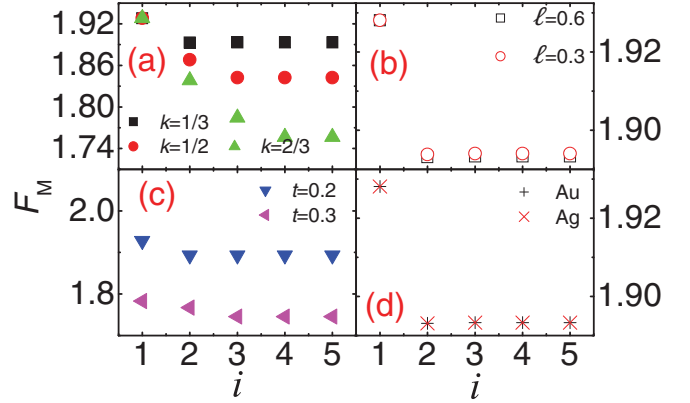FIG. 6. (Color online) Same as in Fig. 4 for the F_E.

FIG. 7. (Color online) Same as in Fig. 5 for the F_M.

that F_M of only a factor of 2 can take place in this MCSN array.

Before we go into more detail, we make some comments on earlier similar studies. The F_E of MCSNs was first reported by LSB [9]. The overall features of our data well agree with theirs in this THz region. A self-similar assembly of Au nanoparticles on DNA templates has been demonstrated in Ref. [15]. It was noted in [15] that Mie calculations predict field intensities enhanced by four orders of magnitude in these nanostructures. Reference [30] reported analytical expressions for the electromagnetic magnitudes in touching nanoparticle dimers. Specifically, it was theoretically discussed that nanosphere dimers are highly efficient structures to collect and concentrate broadband radiation, that is, F_E of the order of 10^4, at their touching point. Speaking more generally, we would like to note that our approach is applicable to the description of such singular metal nanostructures. We should mention here that composite plasmonic nanostructures, designed to achieve cascaded enhancement of electromagnetic fields at optical frequencies, demonstrated dramatic enhancement of the Raman signals when compared to those measured from constituent elements [31].

Figures 8(a) and 8(b) show that subwavelength concentration of the electromagnetic field can be achieved in the narrow gap separating nanoparticles near the smallest nanodisk. This observation is consistent with the earlier report of LSB [9] and a series of recent studies [32]. To solidify this assertion and for illustrative purposes, we estimate a focusing length Ξ which represents the distance over which F_E attains 85% of its maximum value. It scales (not shown) with i as $\propto \exp(-\chi i)$, where χ is a constant which is the same for the electric excitation at PLR and the magnetic excitation at GYR. To obtain additional information about the focusing efficiency of the MCSNs, we have plotted $(\Xi/\lambda)_{PLR}$ against F_E. We find that it decreases with F_E [Fig. 9(a)], giving the approximate scaling law $(\Xi/\lambda)_{PLR} \propto F_E^{-1.5}$, suggesting a power-law behavior for describing the locality of plasmon dispersion. A notable feature of the data is the apparent lack of distinction in the -1.5 exponent for different sets of geometric parameters and metal phases of the MCSNs. We checked (not shown) that shifting the threshold up from 85% to 90% of the maximum value of the F_E does not drastically affect the -1.5 exponent. From Fig. 9(a) we also see a good correspondence with the -1.5 exponent for full core nanoparticles ($t = 1$).
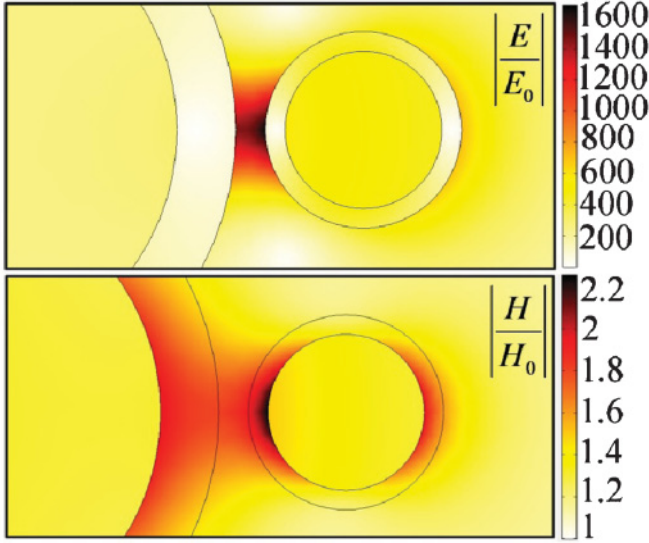
FIG. 8. (Color online) (a) The F_E in the (x-y) plane of the array of MCSNs (fifth iteration). $k = 1/3$, $t = 0.2$, and $l = 0.3$. The metal phase is assumed to be Au. E_x polarization and $\lambda_{PLR} = 923.93$ nm. F_E is defined as the ratio between the modulus of the electric field to the exciting electric field E_0. (b) Same as in Fig. 8 for the F_M. H_x polarization and $\lambda_{GYR} = 66.23$ mm. The exciting magnetic field is $H_0 = 1$ A m^{-1}.

Taken in their totality, our simulation results indicate that this power-law behavior may be a generic feature associated with the focusing efficiency of two-dimensional MCSNs. As a point of comparison, it is important to note that finite-difference time-domain computations demonstrated a nanolens effect which can convert a diffraction limited Gaussian beam into a subwavelength focus as small as $\lambda/10$ for self-similar Ag nanosphere array embedded in glass [32]. This should be contrasted with the plot of $(\Xi/\lambda)_{GYR}$, defined as the distance over which F_M attains 81% of its maximum value, versus F_M [Fig. 9(b)]. The overall conclusion from Fig. 9(b) is rather encouraging: It appears to be possible to concentrate a modest magnetic field over a subwavelength spatial extent $\approx \lambda/10^7$ in the microwave regime. This result also indicates that the different focusing length dependences of the field enhancement arise from decoupled mechanisms, as expected for irrotational electric and magnetic fields in the heterostructures [13].

IV. SUMMARY

To summarize, we have reported a systematic study of the electromagnetic material properties of a canonical model of self-similar nanostructures in which the near fields produced by an illuminated large MCS nanoparticle play the role of the exciting field for smaller MCS nanoparticles. The results presented here, which are based on FE calculations and a set of reasonable assumptions, provide insight into the study of the microwave and optical properties of MCSNs. The treatment here extends the study of LSB in several respects: Additional control parameters are considered, and GYR properties are discussed. Our results are also consistent with those of Foteinopoulou *et al.* [33] on a tapered self-similar Ag nanosphere array (see Figs. 7(b) and 8(b) of [33]). The
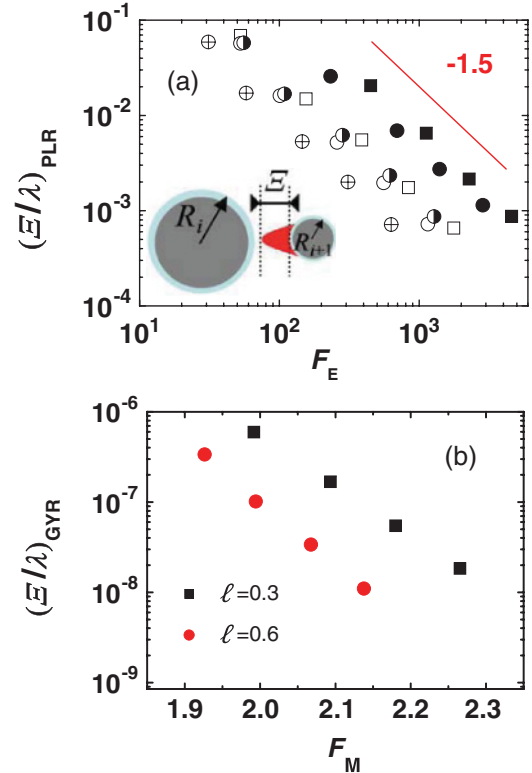

FIG. 9. (Color online) (a) The relative focusing length, Ξ/λ, with respect to the PLR wavelength of the excitation, as a function of F_E for the array of MCSNs. E_x polarization. $k = 1/3$. ○: $t = 0.2$, $l = 0.6$; the metal phase is assumed to be Au. □: $t = 0.2$, $l = 0.3$; the metal phase is assumed to be Au. ◗: $t = 0.3$, $l = 0.6$; the metal phase is assumed to be Au. ⊕: $t = 0.2$, $l = 0.6$; the metal phase is assumed to be Ag. For the purpose of comparison, the case of full core ($t = 1$) is also considered. The metal phase is assumed to be Au. ■: $l = 0.3$; the metal phase is assumed to be Au; ●: $l = 0.6$. (b) Same as in (a) for the GYR. $k = 1/3$. Squares: $t = 0.2$, $l = 0.3$. Circles: $t = 0.2$, $l = 0.6$. The metal phase is assumed to be Au and H_x polarization is considered.

localized character behavior of the PLR to the nanostructure results in the strong field concentration, of the order of 10^3, as is apparent in Fig. 6. Based on these results, we demonstrate the broadband nanolens capability of the MCSN array. We have defined a focusing length which is exponentially sensitive to the iteration number of the MCSNs. The results described above demonstrate that F_E and focusing length are related by a scaling law. This insight heightens the relevance of systematic searches, experimentally, as well as computationally, for novel nanostructures, allowing us to control the subwavelength concentration of the optical field. A primary motivation for our calculations was to demonstrate the localized character of the field enhancement capabilities which are crucial for plasmon sensor applications, that is, surface plasmon sensing using clusters of nanoparticles coated with biomolecules [34]. Beyond its intrinsic interest, the sum of these observations supports the view that the large tunability of the quasielectrostatic properties of such hybrid nanostructures with many more degrees of freedom compared to a single-phase material can have important implications for magnetic-photonic device applications. Other themes such as focusing properties of

three-dimensional self-similar anisotropic MCSNs, assembly of MCSNs into random arrays or superlattices [35], calculations of the scattering and absorption efficiencies of MCSNs [36], and subwavelength imaging [37] would also be natural extensions of the present work.

[1] S. A. Maier, *Plasmonics: Fundamental and Applications* (Springer, New York, 2007).

[2] H. Raether, *Excitations of Plasmons and Interband Transitions by Electrons* (Springer Verlag, Berlin, 1980); see also H. Raether, *Surface Plasmons on Smooth and Rough Gratings* (Springer, Berlin, 1988); *Surface Plasmon Nanophotonics*, edited by M. L. Brongersma and P. G. Kik (Springer, Dordrecht, 2007); *Nanophotonics with Surface Plasmons*, edited by V. M. Shalaev and S. Kawata (Elsevier, Amsterdam, 2007).

[3] M. I. Stockman, S. V. Faleev, and D. J. Bergman, Phys. Rev. Lett. **87**, 167401 (2001).

[4] W. L. Barnes, A. Dereux, and T. W. Ebbesen, Nature (London) **424**, 824 (2003).

[5] E. Ozbay, Science **311**, 189 (2006); C. S. Levin, C. Hofman, T. A. Ali, A. T. Kelly, E. Morosan, P. Nordlander, K. H. Whitmire, and N. J. Halas, ACS Nano **3**, 1379 (2009); W. Chen, N. Xu, L. Xu, L. Wang, Z. Li, W. Ma, Y. Zhu, C. Xu, and N. A. Kotov, Macromol. Rapid Commun. **31**, 228 (2010).

[6] L. Novotny, Phys. Rev. Lett. **98**, 266802 (2007); P. Bharadwaj, B. Deutsch, and L. Novotny, Adv. Opt. Phot. **1**, 438 (2009).

[7] S. I. Bozhevolny (editor), *Plasmonic Nanoguides and Circuits* (World Scientific, Singapore, 2008).

[8] P. Mühlschlegel, H. J. Eisler, O. J. F. Martin, B. Hecht, and D. W. Pohl, Science **308**, 1607 (2005).

[9] K. Li, M. I. Stockman, and D. J. Bergman, Phys. Rev. Lett. **91**, 227402 (2003).

[10] J. Takahara, S. Yamagishi, H. Taki, A. Morimoto, and T. Kobayashi, Opt. Lett. **22**, 475 (1997).

[11] D. A. Genov, A. K. Sarychev, V. M. Shalaev, and A. Wei, Nano Lett. **4**, 153 (2004); V. M. Shalaev, Phys. Rep. **272**, 61 (1996); *Properties of Nanostructured Random Media*, edited by V. M. Shalaev (Springer, New York, 2002); J. Borneman, K.- P. Chen, A. Kildishev, and V. Shalaev, Opt. Express **17**, 11607 (2009); J. Li, A. Salandrino, and N. Engheta, Phys. Rev. B **76**, 245403 (2007).

[12] M. Quinten, A. Leitner, J. R. Krenn, and F. R. Aussenegg, Opt. Lett. **23**, 1331 (1998).

[13] M. Essone Mezeme, S. Lasquellec, and C. Brosseau, Phys. Rev. E **81**, 057602 (2010).

[14] M. Essone Mezeme, S. Lasquellec, and C. Brosseau, J. Appl. Phys. **109**, 014302 (2011).

[15] S. Bidault, F. Javier Garcia de Abajo, and A. Polman, J. Am. Chem. Soc. **130**, 2750 (2008).

[16] M. A. Ordal, L. L. Long, R. J. Bell, S. E. Bell, R. R. Bell, R. W. Alexander Jr., and C. A. Ward, Appl. Opt. **22**, 1099 (1983).

[17] S. B. Ni, S. M. Lin, Q. T. Pan, F. Yang, K. Huang, and D. Y. He, J. Phys D **42**, 055004 (2009); J. Ben Youssef and C. Brosseau, Phys. Rev. B **74**, 214413 (2006); C. Brosseau and P. Talbot, IEEE Trans. Dielectr. Electr. Insul. **11**, 819 (2004); J. Appl. Phys. **97**, 104325 (2005); C. Brosseau, J. Ben Youssef, P. Talbot, and A.- M. Konn, *ibid*. **93**, 9243 (2003); M. Pardavi-Horvath

and L. J. Swartzendruber, IEEE Trans. Magn. **35**, 3502 (1999); M. Pardavi-Horvath, G. Zheng, and G. Vertery, Physica B **233**, 287 (1997).

[18] M. Marklund, G. Brodin, L. Stenflo, and C. S. Liu, Europhys. Lett. **84**, 17006 (2008).

[19] E. Townsend and G. W. Bryant, in *Quantum Electronics and Laser Science Conference*, OSA Technical Digest (CD) (Optical Society of America, 2011), paper QThC2.

[20] I. V. Antonets, L. N. Kotov, S. V. Nekipelov, and Ye. A. Golubev, translated from Zhurnal Tekhnichesko Ĭ Fiziki **74**, 102 (2004) [Tech. Phys. **49**, 1496 (2004)].

[21] H. Xu, Appl. Phys. Lett. **87**, 066101 (2005); see also J. Enderlein, *ibid*. **87**, 066102 (2005); K. Zhao, H. Xu, B. Gu, and Z. Zhang, J. Chem. Phys. **125**, 081102 (2006); H. Xu, Phys. Rev. B **72**, 073405 (2005); J. Opt. Soc. Am. A **21**, 804 (2004); Phys. Lett. A **312**, 411 (2003).

[22] H. Hövel, S. Fritz, A. Hilger, U. Kreibig, and M. Vollmer, Phys. Rev. B **48**, 18178 (1993).

[23] P. Stoller, V. Jacobsen, and V. Sandoghdar, Opt. Lett. **31**, 2474 (2006).

[24] COMSOL MULTIPHYSICS version 3.4, [http://www.comsol.com].

[25] F. J. Garcia de Abajo, J. Phys. Chem. C **112**, 17983 (2008).

[26] A. Mejdoubi and C. Brosseau, Phys. Rev. E **74**, 031405 (2006).

[27] J. B. Khurgin and G. Sun, J. Opt. Am. Soc. B **26**, B83–B95 (2009); A. Aubry, D. Y. Lei, S. A. Maier, and J. B. Pendry, Phys. Rev. Lett. **105**, 233901 (2010).

[28] P. Nordlander and C. Oubre, Nano Lett. **4**, 899 (2004).

[29] M.- W. Chu, V. Myroshnychenko, C. H. Chen, J.-P. Deng, C.-Y. Mou, and F. Javier García de Abajo, Nano Lett. **9**, 399 (2009).

[30] A. I. Fernández-Domínguez, S. A. Maier, and J. B. Pendry, Phys. Rev. Lett. **105**, 266807 (2010).

[31] V. G. Kravets, G. Zoriniants, C. P. Burrows, F. Schedin, C. Casiraghi, P. Klar, A. K. Geim, W. L. Barnes, and A. N. Grigorenko, Phys. Rev. Lett. **105**, 246806 (2010).

[32] J. P. Kottman and O. J. F. Martin, Opt. Express **8**, 655 (2001); E. Hao and G. C. Scatz, J. Chem. Phys. **120**, 357 (2004).

[33] S. Foteinopoulou, J. P. Vigneron, and C. Vandenbeml, Opt. Express **15**, 4253 (2007); See also S. E. Sburlan, L. A. Blanco, and M. Nieto-Vesperinas, Phys. Rev. B **73**, 035403 (2006).

[34] D. Pissuwan, S. M. Valenzuela, and M. B. Cortie, Trends Biotechnol. **24**, 62 (2006).

[35] C. S. Levin, C. Hofmann, T. A. Ali, A. T. Kelly, E. Morosan, P. Nordlander, K. H. Whitmire, and N. J. Halas, ACS Nano **3**, 1379 (2009); W. L. Zhou, E. E. Carpenter, J. Lin, A. Kumbhar, J. Sims, and C. J. O'Connor, Eur. Phys. J. D **16**, 289 (2001).

[36] A. Mejdoubi, M. Essone Mezeme, Z. Sekkat, M. Bousmina, and C. Brosseau, (unpublished).

[37] X. Huang, S. Xiao, D. Ye, J. Huangfu, Z. Wang, L. Ran, and L. Zhou, Opt. Express **18**, 10377 (2010).